NUMERICAL SIMULATION AND ANALYSIS OF PHASE CHANGE HEAT TRANSFER IN CRUDE-OIL

by

Ying XU[a], Xin NIE[a*], Zhonghua DAI[b], Xiao-Yan LIU[a*], Yang LIU[a], and Qinglin CHENG[1,a]

[a] Northeast Petroleum University, Daqing City, China
[b] Daqing Oilfield Company No.3 Oil Production Plant, Daqing City, China

Original scientific paper
https://doi.org/10.2298/TSCI190623464X

Accurately obtaining the temperature distribution of the medium in the shutdown pipe-line of waxy crude-oil has important guiding significance for making maintenance plan and restart plan. The phase transition process of waxy crude-oil involves complex problems such as natural-convection heat transfer, latent heat release, and difficulty in tracing liquid-solid interface. In this paper, the concept and significance of breaking point were proposed. Taking the breaking point and the freezing point as dividing point, a new zonal partition model was established based on the influence of phase change of crude-oil wax crystal on heat transfer mode, with the corresponding governing equations being established for different regions. With the proposed model, the effects of natural-convection on heat transfer, latent heat release, location change of condensate reservoir, heat transfer mechanism, and other key issues in the process of oil phase transition were analyzed.

Key words: *phase change, waxy crude-oil, heat transfer, numerical simulation, condensate reservoir*

Introduction

Waxy crude-oil has a wide temperature range because of its complex wax composition. It is important to describe the heat transfer characteristics in the process of phase transition and to obtain the temperature distribution of crude-oil at different stoppage times. The research of wax and other phase change materials has been relatively mature [1-5], but for the complex component of crude-oil, the phase change heat transfer research needs to be further developed.

How to describe the natural-convection heat transfer in the process of phase transition is one of the key problems in obtaining accurate temperature field [6-9]. In the early models [10-13], natural-convection heat transfer was neglected, and the liquid-solid two-phase partition was adopted, and an equivalent thermal conductivity equation was established in the liquid phase region, the influence of natural-convection on heat transfer process cannot be analyzed by this method. For the liquid-solid two-phase partition model, latent heat was considered to be completely released at an infinitely thin phase interface [14, 15].

With the development of DSC technology, latent heat was transformed into variable specific heat capacity, and equivalent specific heat capacity is used to describe the heat transfer process in the governing equation [16-20]. This treatment of latent heat of phase change

[*] Corresponding authors, e-mail: niexin2592@sina.com; liu_xydq@163.com

was a reasonable and feasible way to accurately represent the latent heat release at different temperatures.

In fact, after the temperature of wax-containing crude-oil drops to the wax point, wax precipitation and latent heat release begin. In the initial stage, a small amount of wax crystals are suspended in the liquid phase crude-oil. Subsequently, when the amount of wax crystals increases continuously, a grid structure will be formed through gelling [10, 21-26]. Therefore, there is a liquid-solid mixed fuzzy zone in the process of phase transition in the pipe-line, which can be regarded as porous medium. For this fuzzy region, most scholars used enthalpy-porous media model to describe heat transfer and flow [27-30]. In the aforementioned models, Darcy formula was used to describe the natural-convection of liquid phase in the pores. The release of crude-oil latent heat of wax appearance was considered as occurring in a narrow temperature zone near the freezing point [29, 30]. However, there was no explanation regarding determination of these temperature ranges.

When the temperature of crude-oil is lower than the abnormal point, the crude-oil has non-Newtonian characteristics, and the viscosity of crude-oil varies significantly with temperature and shear rate [31-33]. For the non-Newtonian properties, most scholars used the viscosity change characterization [15, 20]. In Xu's models, momentum equations were established, respectively for Newtonian fluid and non-Newtonian fluid, with the influence of crude-oil viscosity change on the shutdown process being analyzed, and the final results show that the influence of viscosity change on the shutdown pipe-line can be ignored [34].

In this paper, combined with the influence of the phase change of wax crystal on the heat transfer process in the process of wax evolution in crude-oil, a new zonal mathematical model will be established to describe the heat transfer characteristics of crude-oil phase transition more accurately. Based on the new model, the effects of natural-convection on heat transfer, latent heat release, location change of condensate reservoir, heat transfer mechanism and other key issues in the process of oil phase transition will be analyzed in depth, so as to enrich the heat transfer mechanism of oil.

Physical model

The physical model of an overhead pipe-line in shutdown was shown in the fig. 1. From the inside to the outside, there were crude-oil, steel pipe and insulation layer.

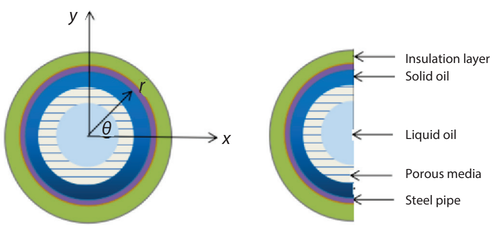

Figure 1. Physical model for an overhead pipe-line

Phase change and heat transfer of wax crystal

In the process of crude-oil cooling, the phase state of crude-oil can be divided into four stages:

- When the oil temperature is higher than the wax point, the crude-oil in the whole pipe-line is liquid phase crude-oil, which is in the stage of natural-convection heat transfer.
- When the temperature of crude-oil is lower than the wax point, a small amount of wax crystals will be precipitated out and suspended in the liquid phase. At this time, due to the small amount of wax crystals, the presence of wax crystals will not affect the change of heat transfer mode of the main body in the pipe-line.
- When the wax crystal precipitates about 2%, it will form a cementitious structure [35, 36]. At this time, the crude-oil can be regarded as porous medium, and the heat transfer mode is

natural-convection heat transfer in the liquid phase crude-oil in the void, and the wax crystal is mainly thermal conduction mode.

– When the temperature of crude-oil drops to the freezing point, it can be regarded as a pure solid phase, and its heat transfer mode is heat conduction.

Definition and significance of breaking point

It can be seen from the previous analysis that the heat transfer modes in the first and second stages are natural-convection heat transfer, which can be described by the same model. Therefore, they are all regarded as *liquid phase regions*. When the amount of wax crystal increases to a grid structure, the corresponding temperature is *the breaking point temperature*, and it can be regarded as the temperature point at which the porous medium is formed.

Assumptions

In order to simplify the calculation, there were some assumptions:

– neglecting viscous dissipation in the fluid,
– the medium in the pipe is incompressible fluid, and
– at the beginning of shutdown, the temperature of crude-oil is consistent throughout the pipeline.

Mathematical model

Liquid zone

The governing equations in the liquid phase region include the continuity equation (1), the momentum equation (2), and the energy equation (3):

$$\frac{\partial \rho}{\partial t}+\mathrm{div}(\rho u)=0 \tag{1}$$

$$\frac{\partial(\rho u)}{\partial t}+(\rho u\nabla)u=-(\nabla P)+(\nabla\tau)+F \tag{2}$$

$$\frac{\partial(\rho u)}{\partial t}+\mathrm{div}(\rho uu)=-\frac{\partial P}{\partial x}+\frac{\partial\tau_{xx}}{\partial x}+\frac{\partial\tau_{yx}}{\partial y}+F_x \tag{2a}$$

$$\frac{\partial(\rho v)}{\partial t}+\mathrm{div}(\rho vu)=-\frac{\partial P}{\partial y}+\frac{\partial\tau_{xx}}{\partial x}+\frac{\partial\tau_{yy}}{\partial y}+F_y \tag{2b}$$

$$\tau_{xx}=2\mu\frac{\partial u}{\partial x}+\lambda\mathrm{div}(u) \tag{2c}$$

$$\tau_{yy}=2\mu\frac{\partial v}{\partial y}+\lambda\mathrm{div}(u) \tag{2d}$$

$$\tau_{xy}=\tau_{yx}=\mu\left(\frac{\partial u}{\partial y}+\frac{\partial v}{\partial x}\right) \tag{2e}$$

$$\lambda=-\frac{2}{3}\mu \tag{2f}$$

In the momentum eq. (2), F is the source term of the external force, which includes the components in the X- and Y-directions, $F_x = 0$, and $F_y = -\rho$g.

$$\frac{\partial(\rho c_p T)}{\partial t}+(\rho c_p u\nabla T)=\lambda_t\nabla^2 T \tag{3}$$

When oil temperature is higher than the wax precipitation point, $\lambda_t = \lambda_l$, and when the oil temperature is between breaking point and wax precipitation point, λ_t, is determined:

$$\varepsilon = 1-\frac{T_x - T}{T_x - T_n} \tag{3a}$$

$$\phi = 1-\varepsilon \tag{3b}$$

$$\lambda_t = \lambda_l \frac{2+\dfrac{\lambda_s}{\lambda_l}+2\phi\left(\dfrac{\lambda_s}{\lambda_l}-1\right)}{2+\dfrac{\lambda_s}{\lambda_l}-\phi\left(\dfrac{\lambda_s}{\lambda_l}-1\right)} \tag{3c}$$

Solid zone

The governing equation of the solid phase region is the energy equation, as shown in the formula (3), where $\lambda_t = \lambda_l$.

Liquid-solid mixed porous media zone

In the porous media range, Brinkmann-Forchheimer-Darcy porous media seepage model is adopted, where, permeability, K, shape factor, F_s, and equivalent thermal conductivity, λ_t are determined by liquid phase rate calculation:

$$\frac{\partial(\rho u)}{\partial t}+(\rho u\nabla)\frac{u}{\varepsilon} = -\nabla(\varepsilon P)+\mu_e\nabla^2 u + F \tag{4}$$

$$F = -\frac{\varepsilon\mu_e}{K}u\rho - \frac{\varepsilon F_\varepsilon}{\sqrt{K}}u|u| + \varepsilon\rho g\beta(T-T_{\text{ref}}) \tag{4a}$$

$$F_\varepsilon = \frac{1.75}{\sqrt{150\varepsilon^3}} \tag{4b}$$

$$K = \frac{\varepsilon^3}{C(1-\varepsilon)^2} \tag{4c}$$

$$\lambda_t = (1-\varepsilon)\lambda_s + \varepsilon\lambda_l \tag{4d}$$

Piping and insulation

The heat transfer equations of steel pipe and insulation material:

$$\rho_p c_{1p}\frac{\partial T}{\partial t} = \lambda_1\left(\frac{\partial^2 T}{\partial x^2}+\frac{\partial^2 T}{\partial y^2}\right),\; r_1 \le \sqrt{x^2+y^2} \le r_2 \tag{5}$$

$$\rho_\text{i} c_\text{i}\frac{\partial T}{\partial t} = \lambda_2\left(\frac{\partial^2 T}{\partial x^2}+\frac{\partial^2 T}{\partial y^2}\right),\; r_2 \le \sqrt{x^2+y^2} \le r_3 \tag{6}$$

Boundary and initial conditions

$$-\lambda_1 \frac{\mathrm{d}t}{\mathrm{d}r}\bigg|_{r=r_3} = h(T - T_f),\ \sqrt{x^2+y^2} = r_3 \tag{7}$$

$$T\big|_{t=0} = cons\tan t \tag{8}$$

Verification and analysis

The SIMPLE algorithm was adopted for simulation. The independence of the grid number and time step was verified. First, three models with grid numbers of 10100, 29765, and 59311 were simulated, and the curve of the average temperature of crude-oil in the tube with time for different grid numbers was compared. The results were as followed in fig. 2. It can be found that the temperature drop curve with the number of grids of 10100 was obviously different from other curves, and the temperature drop curves of crude-oil with the number of grids of 29765 and 59311 almost overlap, so it can be determined that 29765 was the appropriate number of grids. The calculation accuracy of the model had reached the maximum, and increasing the number of grids basically had no effect.

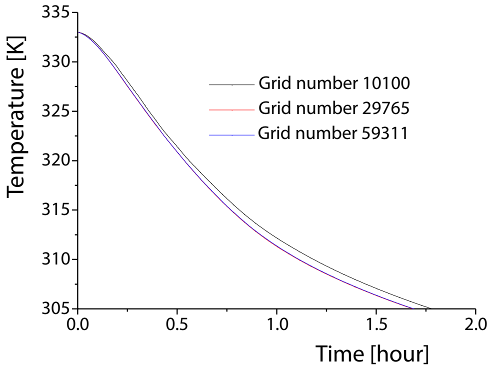

Figure 2. Average temperature drop curves of pipe-lines with different mesh numbers

Then, the model was verified with time step for the grid number of 29765, and the curves of the average temperature in the pipeline with time steps of 60 seconds, 40 seconds, 20 seconds, and 10 seconds were compared, as shown in fig. 3. The temperature drop curve showed a clear tendency to converge as the time step decreases, until the time step of 20 seconds. Also, the temperature drop curve at the step of 20 seconds and the step of 10 seconds basically overlap, so it can be determined that 20 seconds was the appropriate time step of the 29765 grid number model.

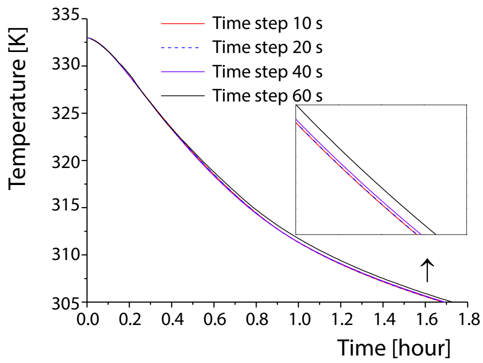

Figure 3. Average temperature drop curves of pipe-lines with different time steps

The pipe was bare without insulation layer, and the air temperature was held constant at 290 K. The experimental crude-oil was from the oil field site in Daqing city, with the wax precipitation temperature of 319 K, the breaking point of 313 K and the freezing point of 305 K. Physical parameters of crude-oil steel pipe were listed in tab. 1. The experimental flow diagram was shown in the fig. 4.

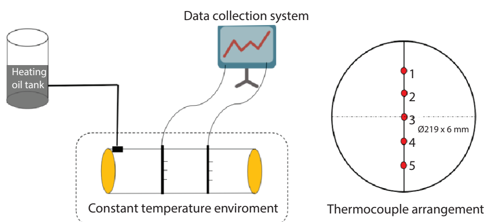

Figure 4. Experimental diagram

Table 1. Experimental crude-oil parameters

Parameter	Units	Value
Oil density, ρ	[kgm^{-3}]	$\rho = 0.902 - 8.177 \cdot 10^{-4}(T - 273.15) + 1.54 \cdot 10^{-6}(T - 273.15)^2$ (9)
Oil thermal conductivity, λ	[Wm^{-1}K^{-1}]	$\lambda_l = 0.15,\ T > 315\,\text{K}$ $\lambda_s = 0.25,\ T < 310\,\text{K}$ (10)
Oil dynamic viscosity, μ	[Pa·s]	For Newtonian fluid: $\mu = 10^{5.06039-0.01951T},\ T \ge T_1$ (11) non-Newtonian fluid: $\mu = \begin{cases} 10^{37.30785-0.12235T}, & T_2 \le T < T_1 \\ 10^{-14.44979+0.0511T}, & T_3 \le T < T_2 \\ 10^{20.81207-0.06799T}, & T_4 \le T < T_3 \end{cases}$ (12) $T_1 = 313.15$ K, $T_2 = 298.15$ K, $T_3 = 296.15$ K, $T_4 = 292.15$ K
Specific heat of oil	[JK^{-1}kg^{-1}]	$c_p = \begin{cases} 2140 & T \ge 322\,\text{K} \\ -35.8T + 13667.5 & 303.15\,\text{K} \le T < 322\,\text{K} \\ 18.33T - 2737.75 & 273.15\,\text{K} \le T < 303.15\,\text{K} \end{cases}$
Density of steel pipe	[kgm^{-3}]	7850
Specific heat of steel pipe	[JK^{-1}kg^{-1}]	500
Conductivity of steel pipe	[Wm^{-1}K^{-1}]	48
Dimensions/size of steel pipe	[mm]	219×7

The crude-oil was heated to 333 K in a heating tank and then entered a 0.5 m long experimental tube with a 60 mm insulation material at both ends. Automatically closed the tank valve when the level gauge showed full tube. Two monitoring positions were arranged on the pipe-line, and five monitoring points were set at each position. The external environment of the pipe-line was at a constant temperature of 290 K. Heating tank temperature control device, thermocouple, level gauge, temperature sensor and other instruments all had been calibrated, the test accuracy can reach ±2%. The experimental results were taken as the arithmetic mean value of the corresponding positions at the two monitoring points. Shutdown process under experimental conditions was calculated by proposed model. The experimental and simulated results of crude-oil temperature at typical locations were shown in tab. 2.

Table 2. Comparison between the test data and calculated results

	5 point			3 point			2 point		
Time [minute]	Cal	Test	Relative error	Cal	Test	Relative error	Cal	Test	Relative error
5	56.1	55.3	1.42%	58.3	58.8	–0.85%	59	59.5	0.84%
20	51.2	49.4	3.51%	55.3	54.4	1.62%	56.6	56.1	0.88%
40	47.4	46.9	1.05%	50.7	50.0	1.38%	52.2	51.3	1.72%
60	43.6	44.1	–1.14%	46.8	46.9	-0.21%	48.5	47.8	1.44%
80	41	42.1	–2.68%	44.1	44.5	0.90%	45.5	44.9	1.31%
100	39.4	40.3	2.28%	42.5	42.5	0.00%	43.7	42.6	2.51%
120	38.1	39.1	–2.62%	41.4	40.9	1.20%	42.6	41.8	1.87%

Table 1 presented the comparison of the oil temperature profiles at positions 2, 3, and 5. It can be found that the deviation between the calculated results and the test results was satisfactory, with the max relative error of 3.51%. The fig. 5 was the comparison between the test data and calculated results at the pipe center. According to the figure, the two curves were in good agreement. Next, the proposed model was used for numerical simulation analyze the phase change heat transfer process of crude-oil.

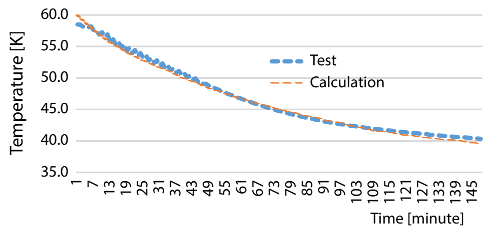

Figure 5. Comparison of temperature drop curve of pipe-line center point

Effect of natural-convection on heat transfer under different pipe diameters

The change of average Rayleigh number in the shutdown process of overhead pipe-lines with different diameters was shown in the fig. 6. The Ra = GrPr, which can indicate the degree of natural-convection.

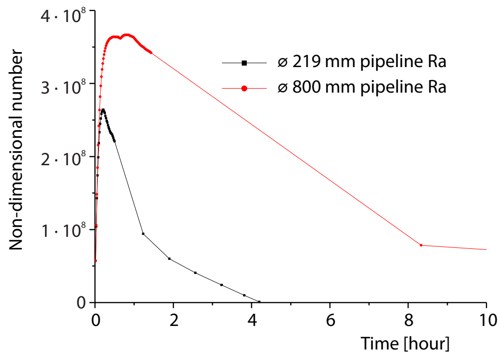

Figure 6. The Rayleigh number change curve

As can be seen from the fig. 6, the trends of the two curves were consistent, in the initial stage of shutdown, Rayleigh number rapidly increased to the peak, and then gradually decreased. The larger the pipe diameter, the higher the peak value of Rayleigh number, this was due to the large diameter pipe-line, its natural-convection space was larger, more fully developed. The peaks of the two pipe diameters were between 10^8 and 10^9, it meant that at the initial stage of shutdown, the natural-convection was in the transition stage of laminar flow turbulence.

When the pipe-line was shutdown for 20 minutes, the distribution of temperature field and flow field in the pipe-line were shown in the fig. 7. For large-diameter pipe-lines, the internal crude-oil content was large and the heat storage capacity was large, so the overall temperature distribution in the pipe-line was higher. For ⌀ 800 mm pipe, the vortex area was larger, the natural-convection was more pronounced, and the effect of natural-convection lasted longer.

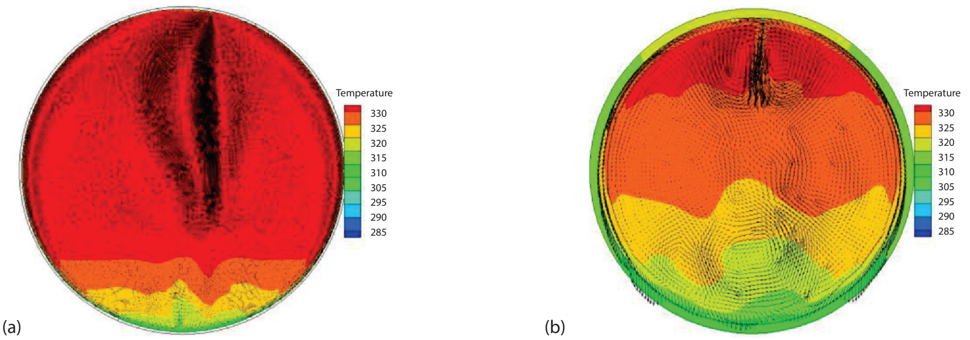

Figure 7. Distribution of temperature field and flow field; (a) 800 mm (20 minutes) and (b) 219 mm (20 minutes)

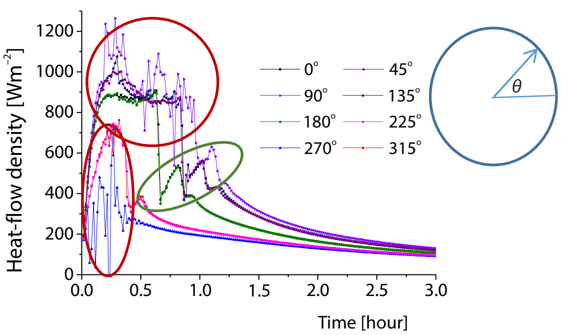

Figure 8. Change in heat flux

Change in heat flux

The fig. 8 showed the heat flux at different positions of the pipe wall.

Because the temperature distribution in the pipe decreased gradually from top to bottom, the maximum heat flux was at the top of the pipe and the minimum was at the bottom wall. Due to the pipe flow field and temperature field on the *Y*-axis approximate symmetrical distribution, as shown in the fig. 6, and, so the heat flux density curves at 45° and 135° coincided, and the pattern was the same at 225° and 315°. Although the curve peaks at different positions were different, the overall change trend was consistent, which can be divided into three stages:

- The period of severe fluctuation was also the initial stage of shutdown (the red part of the coil in fig. 7). At this time, the mixing of cold and hot fluids was severe, and the effect of natural-convection was the most significant.
- As the influence of natural-convection was weakened, the heat flux dropped sharply and then rised slightly, because the latent heat release increased the heat transfer temperature difference.
- Since then, with the appearance of condensate reservoir, the heat flux tended to be consistent at different locations.

Temperature drop and heat transfer characteristic

The temperature distribution on the *Y*-axis of the pipe-line at different shutdown times were shown in the fig. 9.

As can be seen from the fig. 9, the highest temperature point was in the positive *Y*-axis, while the lowest temperature point was in the lowest *Y*-axis at the same shutdown time, this was due to natural-convection, with hot oil moving up and cold oil moving down. With the increase of shutdown time, condensate layer appeared in the inner wall of the pipe-line, and the liquid crude-oil gradually decreases, so the maximum temperature point was gradually close to the center of the pipe, but the final freezing point was above the center of the pipe-line. When the influence of natural-convection can be ignored, the temperature distribution in the pipe was approximately symmetric about the Y-axis.

The crude-oil freezing point was 305 K, and the above the dotted lines in the fig. 9 were all liquid crude-oil regions. The graph can be used to determine the position of condensate reservoir on the Y-axis at a typical shutdown time. For example, when the transmission was shutdown for 1 hour, the temperature of the positive half of the Y-axis was all higher than 305 K, while the temperature of the crude-oil from about 85 mm of the negative half axis to the bottom of the pipe wall was all lower than the condensation point, and the thickness of the condensate reservoir was about 19 mm. When the shutdown lasted for 5 hours, the temperature curve on the entire Y-axis was below 305 K, and the crude-oil in the pipe-line was all solidified. The aforementioned conclusions can be further proved by the fig. 10, which was solidified cloud picture at different shutdown time, and the blue part represented solidified crude-oil.

The curves were spaced 0.5 hours apart, so the density can reflect the temperature drop rate at the corresponding stage. Obviously, the temperature drop rate was the highest at the initial moment of shutdown, this is because the temperature difference between inside and outside the pipe-line was the largest at this stage, and there was natural-convection. For the center of the pipe, namely $Y = 0$, the temperature drop rate went through a process from large to small and then increased. The curve circled by the ellipse showed a marked increase in density due to the release of oil latent heat.

The fig. 11 was the temperature drop curves at typical position on Y^+-axis.

From the fig. 11 we can see that the slope change of temperature drop curves can be divided into four sections. In the first stage, the curve had the highest slope and the fastest temperature drop rate. In the second stage, the rate of temperature drop was slowed down due to latent heat release, and the slope was obviously reduced. In the third stage, the influence of latent

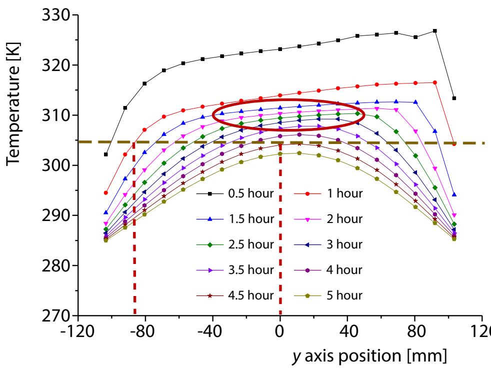

Figure 9. Temperature drop curve on Y-axis

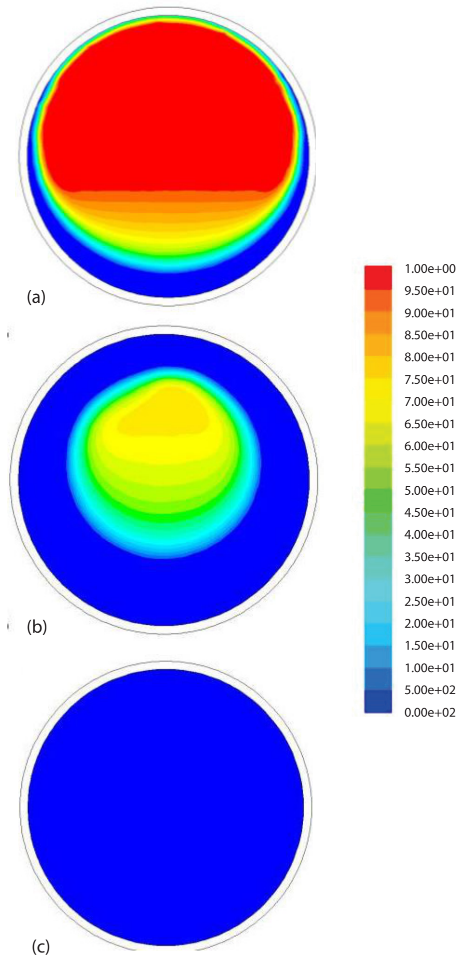

Figure 10. Solidified cloud picture at different shutdown time; (a) 1 hour, (b) 2 hours, and (c) 5 hours

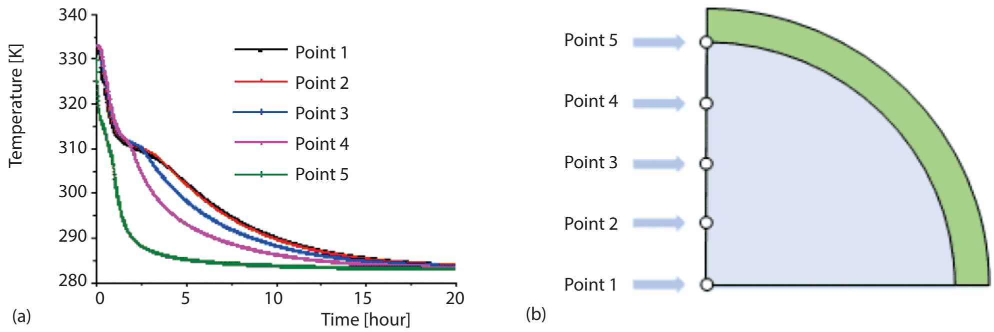

Figure 11. Temperature drop curve at typical position on Y^+-axis

heat was exhausted and the rate of temperature drop increased. As the temperature difference decreased and the thickness of condensate reservoir increased, the temperature drop rate was lower than that in the first stage. In the fourth stage, the crude-oil in the whole pipe-line had all solidified, and the temperature difference was getting lower and lower, and the thermal resistance was large, resulting in a very small slope of the temperature drop curve, which was finally 0.

According to the curves in the fig. 10, for different positions, the latent heat influence duration in the second stage of the temperature drop curve were different. The thermal resistance at the pipe wall was the minimum, so the latent heat released by wax precipitation was much smaller than the heat lost to the outside of the pipe. Compared with other positions, the slope in the second stage was extremely high, and the temperature at this point dropped rapidly to the ambient temperature. According to the comparison of curves, the closer the center was, the more significant the influence of latent heat was.

Conclusions

A new partition model was established,with the latent heat being treated as an additional specific heat capacity. Compared with the experimental results, the maximum relative error was 3.12%, and the agreement was good.

- For overhead pipe-lines with different diameters, the changes of flow field, temperature field and Rayleigh number in the pipe-line after shutdown were analyzed. The results showed that natural-convection develops more fully and the influence of convection heat transfer lasted longer.
- Due to the approximate *Y*-axis distribution of the flow field and the temperature field, the heat flux at the symmetric points on both sides of the *Y*-axis was approximately equal. Because of natural-convection, the heat flux in the whole pipe decreased gradually from top to bottom. The trend of heat flux curve reflected the influence of natural-convection and latent heat release.
- The heat transfer process and characteristics of phase change were described by the temperature distribution curve of *Y*-axis and the solidification cloud diagram.With the extension of shutdown time and the increase of condensate thickness, the highest temperature point in the pipe-line was gradually close to the center of the pipe-line, but the final freezing point was above the center of the pipe-line.
- The temperature drop curves at typical positions on Y^+-axis were used to analyze the influence of latent heat release on temperature drop rate. The results showed that the closer to the pipe wall, the smaller the thermal resistance was, the faster the heat dissipation was, and the less obvious the influence of latent heat was.

Acknowledgment

This work was supported by the National Natural Science Foundation of China (No. 51534004), and Youth Science Foundation of Northeast Petroleum University (2018GPZD-01 and 2018QNL-15).

Nomenclature

C – coefficient, (= $10^4 \cdot 10^7$)
c_i – specific heat capacity of insulating layer, [Jkg^{-1}K^{-1}]
c_p – specific heat capacity of crude-oil, [Jkg^{-1}K^{-1}]
c_{1p} – specific heat capacity of pipe, [Jkg^{-1}K^{-1}]
g – gravitational acceleration, [ms^{-2}]
F – force, [N]
F_ε – shape factor
h – comprehensive heat transfer coefficient, [Wm^{-2}K^{-1}]
K – permeability
P – apparent stress, [Pa]
r_1 – pipe radius, [m]
r_2 – outer radius of pipe/inner radius of insulation material, [m]
r_3 – outside radius of insulation, [m]
T – oil temperature, [K]
T_{ref} – reference temperature, [K]
T_n – freezing point, [K]
T_x – wax precipitation point temperature, [K]
t – shutdown time, [hour]
U – velocity, [ms^{-1}]

Greek symbols

β – expansion coefficient, [K^{-1}]
ε – liquid fraction
λ_1 – pipe thermal conductivity, [Wm^{-1}K^{-1}]
λ_2 – thermal conductivity of insulation, [Wm^{-1}K^{-1}]
λ_l – thermal conductivity of liquid crude-oil, [Wm^{-1}k^{-1})]
λ_s – thermal conductivity of liquid crude-oil, [Wm^{-1}K^{-1}]
λ_t – effective thermal conductivity, [Wm^{-}1K^{-1}]
μ – dynamic viscosity, [kg(ms)$^{-1}$(pa·s)$^{-1}$]
ρ – oil density, [kgm^{-3}]
ρ_{i} – insulating layer density, [kgm^{-3}]
ρ_p – pipe density, [kgm^{-3}]
ϕ – solid fraction

References

[1] Almsater S, *et al*., Development and Experimental Validation of a CFD Model for PCM in a Vertical Triplex Tube Heat Exchanger, *Applied Thermal Engineering*, *116* (2017), Apr., pp. 344-354
[2] Ramalingam, S., Effect of Uniform and Variable Fin Height on Charging and Discharging of Phase Change Material in a Horizontal Cylindrical Thermal Storage, *Thermal Science*, *23* (2019), 3B, pp. 1981-1988
[3] Korawan, A. D., et al., The 3-D Numerical and Experimental Study on Paraffin Wax Melting in Thermal Storage for the Nozzle-and-Shell, Tube-and-Shell, and Reducer-and-Shell Models, *Modelling and Simulation in Engineering*, *2017* (2017), ID 9590214
[4] Stetina, J., et al., Melting Front Propagation in a Paraffin-Based Phase Change Material: Lab-Scale Experiment and Simulations, *Thermal Science*, *22* (2018), 6B, pp. 2723-2732
[5] Mao, Q. J., *et al*., A Novel Heat Transfer Model of a Phase Change Material Using in Solar Power Plant, *Applied Thermal Engineering*, *129* (2018), Jan., pp. 557-563
[6] Sassos, A., Pantokratoras, A., *et al.,* Convection in the Rayleigh-Benard Flow with all Fluid Properties Variable, *Journal of Thermal Science*, *5* (2011), 20, pp. 454-459
[7] Li, W., *et al.*, Studies on Temperature Drop of Buried Waxy Crude Pipe-lines in Shutdown: A General Review, *Oil and Gas*, *23* (2004), Sept., pp. 4-8
[8] Yu, G., et al., A New General Model for Phase-Change Heat Transfer of Waxy Crude-Oil during the Ambient-Induced Cooling Proces, Numerical Heat Transfer, *71* (2017), 5, pp. 511-527
[9] Liu, X., *et al*., Study on Heat Transfer Performance of Medium in Aerial Hot Oil Pipe for Shutdown, *Advances in Mechanical Engineering*, *8* (2014), June, pp. 1-7
[10] Zhang, J. J., *et al*., Reliability-Based Approach to the Assessment of Restartability of Waxy Crude Pipelines, *Petroleum Science Bulletin*, *1* (2016), 1, pp. 154-163
[11] Xing, X., A Study of Shutdown and Restart up Process of the Buried Hot Oil Pipe-Line, *Petroleum Planning Aand Engineering*, *12* (2001), 3, pp. 21-23
[12] Han, D. X., *et al*., Fast Thermal Simulation of a Heated Crude-Oil Pipe-Line with a BFC-Based POD Reduced-Order Model, *Applied Thermal Engineering*, *88* (2015), Oct., pp. 217-229

[13] Lee, H. S., *et al*., Waxy Oil Gel Breaking Mechanisms: Adhesive *vs.* Cohesive Failure, *Energy and Fuels*, *22* (2008), 1, pp. 480-487
[14] Li, C. J., Numerieal Analysis of Heated Crude-Oil Pipe-Line at Shutdown, *Oil and Gas Stor Transport*, *20* (2001), 8, pp. 28-31
[15] Chen, J., Xuan, F., Numerical Simulation of the Temperature Drop in Submarine Oil Pipe-Line during Shutdown Based on Fluent, *Journal of Petrochemical Universities*, *27* (2014), Jan., pp. 93-96
[16] Liu, X. Y., *et al*., Melting Experiment of Cuboid Gelled Crude-Oil in Hot Water, *Contemporary Chemical Industry*, *3* (2016), pp. 532-534
[17] Liu, X., *et al.*, Numerical Investigation of Waxy Crude-Oil Paste Melting on an Inner Overhead Pipe Wall, *Applied Thermal Engineering*, *131* (2018), Jan., pp. 779-785
[18] Zhao, Y. S., *et al*., Utilization of DSC, NIR and NMR for Wax Appearance Temperature and Chemical Additive Performance Characterization, *Journal of Thermal Analysis and Calorimetry*, *120* (2015), Feb., pp. 1427-1433
[19] Fan, K. F., *et al*., Determination of the Optimizing Operating Procedure for DSC Test of Wax-Solvent Samples with Narrow and Sharp Wax Peak and Error Analysis of Data Reliability, *Journal Therm. Anal. Calorim.*, *126* (2016), July, pp. 1713-1725
[20] Cheng, Q. L., *et al*., The Study on Temperature Field Variation and Phase Transition Law after Shutdown of Buried Waxy Crude-Oil Pipe-Line, *Case Studies in Thermal Engineering*, *10* (2017), Sept., pp. 443-454
[21] El-Gendy, H., *et al*., The Propagation of Pressure in a Gelled Waxy Oil Pipe-Line as Studied by Particle Imaging Velocimetry, *AIChE Journal*, *58* (2012), 1, pp. 302-311
[22] Peerapornlerd, S., *et al*., Effect of the Flow Shutdown Temperature on the Gelation of Slurry Flows in a Waxy Oil Pipe-Line, *Industrial and Engineering Chemistry Research*, *54* (2015), 16, pp. 4455-4459
[23] Guo, C., *et al.,* Analysis of 2-D Flow and Heat Transfer Modelling in Fracture of Porous Media, *Journal of Thermal Science*, *26* (2017), 4, pp. 331-338
[24] Robustillo, M. D., et al., Assessment of Different Methods to Determine the Total Wax Content of Crude-Oils, *Energy Fuels*, *26* (2012), 10, pp. 6352-6357
[25] Wu, H. H., *et al.*, Numerical Simulation on Typical Parts Erosion of the Oil Pressure Pipe-Line, *Thermal Science*, *17* (2013), 5, pp. 1349-1353
[26] Akgun, M., *et al.*, Experimental Study on Melting/Solidifification Characteristics of a Paraffin as PCM, *Energy Convers Manage*, *48* (2007), 2, pp. 669-678
[27] Wang, M., Yu, *et al*., Numerical Investigation of Melting of the Waxy Crude Oil in an Oil Tank, *Applied Thermal Engineering*., *115* (2017), Mar., pp. 81-90
[28] Yu, G. J., *et al*., Further Study on the Thermal Characteristic of a Buried Waxy Crude Oil Pipe-Line during Its Cooling Process after Shutdown, *Numerical Heat Transfer Part A: Applications*, *71* (2017), 2, pp. 137-152
[29] Lu, T., Jiang, P. X., Heat Transfer Model and Numerical Simulation of Temperature Decreasing and Oil Solidifying of Buried Crude Pipe-Line during Shutdown, *Journal of Thermal Science and Technology*, *4* (2005), Sept., pp. 298-303
[30] Lu, T., Wang, K. S., Numerical Analysis of the Heat Transfer Associated with Freezing/Solidifying Phase Changes for a Pipe-Line Filled with Crude-Oil in Soil Saturated with Water during Pipe-Line Shutdown in Winter, *Journal of Petroleum Science and Engineering*, *62* (2008), 1-2, pp. 52-58
[31] Vinay, G., *et al*., Numerical Simulation of Non-Isothermal Viscoplastic Waxy Crude-Oil Flows, *Journal of Non-Newtonian Fluid Mechanics*, *128* (2005), 2-3, pp. 144-162
[32] Ahmadpour, A., *et al*., The Effect of a Variable Plastic Viscosity on the Restart Problem of Pipe-Lines Filled with Gelled Waxy Crude-Oils, *Journal of Non-Newtonian Fluid Mechanics*, *205* (2014), Mar., pp. 16-27
[33] Pedersen, K. S., Ronningsen, H. P., Influence of Wax Inhibitors in Wax Appearance Temperature, Pour Point, and Viscosity of Waxy Crude-Oils, *Energy Fuels*, *17* (2003), 2, pp. 321-328
[34] Xu, Y., *et al*., Effects of Crude-Oil's Variable Physical Properties on Temperature Distribution in a Shutdown Pipe-Line, *Advances in Mechanical Engineering*, *9* (2017), 5, pp. 1-9
[35] Kane, M., Morphology of Paraffin Crystals in Waxy Crude-oils Cooled in Quiescent Conditions and Under Flow, *Fuel, 82* (2003), 2, pp.127-135
[36] Letoffe, J. M., *et al*., Crude-Oils: Characterization of Waxes Precipitated on Cooling by Dsc and Thermomicroscopy, *Fuel*, *74* (1995), 6, pp. 810-817

Paper submitted: June 23, 2019
Paper revised: December 8, 2019
Paper accepted: December 16, 2019